

# Investigations on the mobility of the glycosidic linkage in sucrose by study of the phase space structure of a two-degrees of freedom model

Giovanna Longhi, Maria Malandrino, and Sergio Abbate

Dipartimento di Scienze Biomediche e Biotecnologie, Università di Brescia, and INFM: UdR, Brescia, Italy

Using the theoretical Ramachandran ( $\phi, \psi$ ) maps reported in the literature for sucrose in vacuo and in aqueous solution, we constructed a two-degrees of freedom model in which the glucose and fructose units are substituted by pseudo-atoms. The complete dynamics of this model is studied numerically at fixed energies. Use is made of the graphic method of the Poincaré surfaces of section in phase space and of the Lissajous maps in configuration space. The reduction to just two degrees of freedom allows one to deal with all initial conditions in phase space, whereas the results of molecular dynamics calculations with all internal degrees of freedoms and with the explicit consideration of solvent molecules are taken into account via effective kinetic and potential energy terms. The conformational isomerization mechanism is investigated by singling out the most reactive trajectories in phase space that are associated with the so-called reactive islands and with the resonances found between the  $\phi$  and  $\psi$  motions. © 2000 by Elsevier Science Inc.

**Keywords:** glycosid linkage, molecular dynamics, Poincaré surfaces of section, conformational isomerization, chaos, reactive islands

## INTRODUCTION

Molecular dynamics (MD) calculations have been employed for a number of years to determine molecular conformations for biological molecules, where free-energy effects are known to be important. Conformations derived in this manner can be

Color Plates for this article are on pages 169–171.

Corresponding author: Sergio Abbate, Dipartimento di Scienze Biomediche e Biotecnologie, Università di Brescia, via Valsabbina 19, 25123 Brescia, Italy. Tel.: +39-0303717415; fax: +39-0303701157.

E-mail address: abbate@med.unibs.it (S. Abbate)

used more confidently than those predicted by molecular mechanics (MM), where only the balance of forces justifies predicted conformations.<sup>1</sup> The use of MD methods is particularly indicated for sugar molecules in solution, where the mobility of OH groups, which tend to form competitive internal and external hydrogen bonds, is crucial for the molecular conformation. Moreover, the mobility of other moieties with low barriers strongly influences the conformation and the most relevant physicochemical properties of the sugar molecules, e.g., the dynamics of the glycosidic linkage, the anomeric effect, and the hexoanomeric effect. These effects, together with a more general treatment of solvation, have been taken into account and investigated by a number of groups.<sup>2–8</sup>

In this and a previous work from our group,<sup>9</sup> we were interested in the mobility of the glycosidic linkage. Such mobility is not influenced by weakly bound electrons, as in the anomeric effect, and the central oxygen is not “engaged” in hydrogen bonds. This allows us, as previously reported,<sup>9</sup> to study the dynamics of the glycosidic linkage using a different approach from that of traditional MD. We have built a two-degrees of freedom model of sucrose ( $\phi$  and  $\psi$  being the two degrees of freedom), in which the glucose and fructose units are replaced by pseudo-atoms, with the same masses as the whole units. In constructing the kinetic and potential energies for our model, we have taken into account the principal characteristics of the conformational properties of the glucose and fructose units and of the glycosidic linkage previously predicted by MD.<sup>3,4</sup> We studied the full vibrational dynamics of this model in the three minima for the conformational energy that were previously predicted.<sup>3,4</sup> Use of graphic methods, such as the Poincaré surfaces of section and the Lissajous maps,<sup>9,10</sup> allows us to draw useful and efficacious pictures of the dynamics of the model. The same methods are employed to investigate the dynamics of the model connecting the three different conformational minima. The role of resonant modes is reported as crucial in leading the reaction of conformational

conversion from one minimum to another. We recall that the role of resonances has been recognized to determine the transition from regular to irregular motions in general dynamical Hamiltonian systems.<sup>10–12</sup> We calculate for our model the most reactive domains in phase space, namely, the reactive islands introduced by Marston and De Leon,<sup>13</sup> to determine where in phase space the trajectories leading to reactions are generated. We will discuss the usefulness of our method in describing qualitatively the isomerization dynamics of the glycosidic linkage. We also will compare our results with those of standard MD calculations.<sup>3,4</sup> Existing MD calculations have been performed with the full glory of the internal degrees of freedom for sucrose, as well as with the inclusion of a number of surrounding water molecules. However, the limitation of those calculations is that they consider few initial conditions, even though the equilibration motion at the beginning of MD calculations accounts for this. We will show that our model nicely complements the results of MD calculations, because it provides results for all possible initial conditions.

## DESCRIPTION OF THE MODEL

As noted in the Introduction, we reduced the dynamics of the glycosidic linkage of the sucrose molecule to only two degrees of freedom, i.e., the torsional internal coordinates  $\phi$  and  $\psi$  of the glucose and fructose units around the  $C_{1g}$ - $O_1$  and  $C_{2f}$ - $O_1$  bonds, respectively. In analogy to our previous work,<sup>9</sup> we introduce two pseudo-atoms  $M_g$  and  $M_f$  to represent the glucose and fructose moieties. We define  $\phi$  as the dihedral angle between the two planes  $M_g$ - $C_{1g}$ - $O_1$  and  $C_{1g}$ - $O_1$ - $C_{2f}$  and  $\psi$  as the dihedral angle formed by  $M_f$ - $C_{2f}$ - $O_1$  and  $C_{2f}$ - $O_1$ - $C_{1g}$  (Figure 1).  $M_g$  and  $M_f$  are defined as follows. The masses of the pseudo-atoms  $M_g$  and  $M_f$  are the total masses of the glucose and fructose units, respectively, excluding the atoms  $C_{2f}$ ,  $O_1$ , and  $C_{1g}$  involved in the glycosidic linkage, i.e., they are both 151 a.m.u. (atomic mass units). The positions of the pseudo-atoms  $M_g$  and  $M_f$  are determined such that the moment of

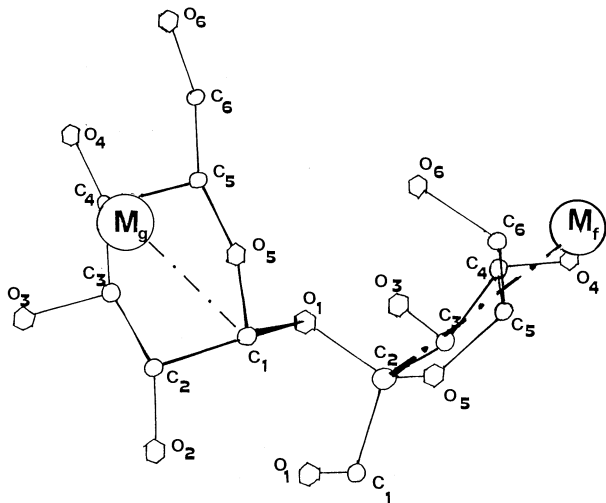


*Figure 1. Schematics of the conformation of sucrose close to equilibrium<sup>3,4</sup> and definition of the positions of pseudo-atoms  $M_g$  and  $M_f$  defined so as to reproduce the moments of inertia of the two molecular rings (see text). The hydrogen atoms are not shown.*

inertia of  $M_g$  with respect to the  $C_{1g}$ - $O_1$  axis is the same as the moment of inertia of the whole glucose unit with respect to it, and the moment of inertia of  $M_f$  with respect to the  $C_{2f}$ - $O_1$  axis is the same as the moment of inertia of the whole fructose unit with respect to it. In so doing, however, we made several assumptions. First, we took the following information from the literature. The crystal structure data from both neutron and X-ray diffraction experiments<sup>14</sup> and the results of MD calculations<sup>3,4</sup> both indicate that the  $^4C_1$  chair is the stable conformation of the pyranoid ring of the glucose unit. The fructose residue shows a higher conformational mobility, but an envelope conformation can be assumed to be prevalent: specifically, the  $^3E$  conformation with the carbon  $C_{3f}$  off the  $C_{2f}$ - $O_{5f}$ - $C_{5f}$ - $C_{4f}$  plane, according to Tran and Brady<sup>3</sup> (Figure 1). In the Ramachandran contour plots calculated previously,<sup>3,4</sup> all minima give forms close to  $^3E$  or intermediate between the two twist forms  $^2^3T$  and  $^4^3T$ . As done previously,<sup>9</sup> we approximate the calculations of the moments of inertia by sticking H and OH groups on the proper carbon atom to which they are bonded, by using CC and CO bond lengths of 1.54 Å and tetrahedral valence angles for glucose (for fructose, all valence angles of the ring are assumed to be tetrahedral except for  $C_2C_3C_4$ ). The model obtained is shown as a stick-and-ball model in Figure 2, together with the definition of the geometric parameters of the model. The precise values for the geometric parameters are listed in Table 1. The orientation of  $M_g$ - $C_{1g}$  is assumed to be that of the line  $C_{1g}$ - $C_{4g}$ , thus giving  $\theta_g = 100^\circ$ ; the orientation of  $M_f$ - $C_{2f}$  is given by the line from  $C_{2f}$  to the center of the opposite bond  $C_{4f}$ - $C_{5f}$ , giving  $\theta_f = 143.85^\circ$ . These angles reflect the property of  $\alpha$ - $\beta$  glycosidic linkage: the axial position of  $C_{1g}$ - $O_1$  and the pseudo-equatorial position of  $C_{2f}$ - $O_1$ . The lengths  $r_g$  of  $M_g$ - $C_{1g}$  and  $r_f$  of  $M_f$ - $C_{2f}$  are fixed so as to reproduce the calculated moments of inertia. We noted that  $r_g$  is shorter than  $r_f$  because  $C_{1g}$ - $M_g$  is nearly perpendicular to the rotational axis  $C_{1g}$ - $O_1$ . The model we built is rather rough; however, it is adequate for our purpose, which is to reproduce general qualitative aspects of the motion of the glycosidic linkage. Having defined the geometry of our model  $M_g$ - $C_{1g}$ - $O_1$ - $C_{2f}$ - $M_f$ , following Decius<sup>15</sup> and our previous work,<sup>9</sup> we can write the coefficients for the kinetic energy, i.e., the G matrix elements relative to the two torsions [ $g(\phi)$  and  $g(\psi)$ ] and the cross term  $g(\phi,\psi)$ . Unlike other reports,<sup>16</sup> we explicitly use the dependence of the G matrix elements from  $\phi$  and  $\psi$ , because we are interested in large-amplitude motions, such as to encompass full conformational changes. The convention for positive torsional angles is taken according to Decius<sup>15</sup>:  $\phi$  is defined as positive if, looking from  $C_{1g}$  to  $O_1$ , clockwise

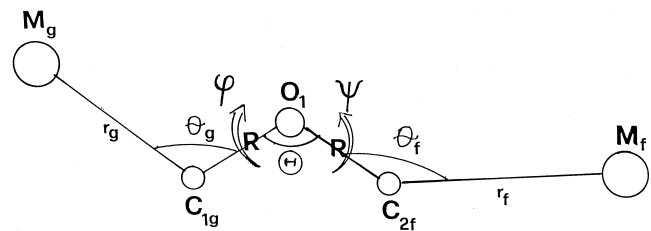


*Figure 2. Model of sucrose employed in the present work with the definition of two degrees of freedom ( $\phi, \psi$ ). The relevant geometric parameters needed for the calculation of the kinetic energy coefficients are defined.*

**Table 1. Geometric characteristics of the model of the present work and values for the parameters of the G elements of Equations 2 (a.m.u.<sup>-1</sup> Å<sup>2</sup>)**

R = 1.54 Å	r <sub>g</sub> = 2.72 Å	r <sub>f</sub> = 3.29 Å		
Θ = 161°	θ <sub>g</sub> = 100°	θ <sub>f</sub> = 143.85°		
K <sub>0</sub> = 0.1434	K <sub>1</sub> = 0.0415	H <sub>0</sub> = 0.1588	H <sub>1</sub> = 0.0598	
J <sub>0</sub> = -0.1084	J <sub>1</sub> = -0.0370	J <sub>2</sub> = -0.0510	J <sub>3</sub> = 0.0006	J <sub>4</sub> = -0.0013

rotation is needed to make M<sub>g</sub> eclipse C<sub>2f</sub>; ψ is positive if, looking from C<sub>2f</sub> to O<sub>1</sub>, clockwise rotation is needed to make M<sub>f</sub> eclipse C<sub>1g</sub>. The Hamiltonian function has the form:

$$H(\varphi, \psi) = \frac{1}{2}g(\varphi)p_{\varphi}^2 + \frac{1}{2}g(\psi)p_{\psi}^2 + g(\varphi, \psi)p_{\varphi}p_{\psi} + V(\varphi, \psi) \quad (1)$$

where p<sub>φ</sub> and p<sub>ψ</sub> are the momenta conjugated to φ and ψ, respectively. The coefficients for kinetic energy g(φ), g(ψ), and g(φ,ψ) are built to guarantee the rototranslational invariance of the whole molecule with all vibrational degrees of freedom.<sup>16</sup> However, we adopt them for our model too.<sup>9</sup> Their functional dependence from φ and ψ is in the simple form of polynomials in sines and cosines of the two angles φ and ψ, namely:

$$g(\varphi) = K_0 + K_1 \cos \varphi \quad (2a)$$

$$g(\psi) = H_0 + H_1 \cos \psi \quad (2b)$$

$$g(\varphi, \psi) = J_0 + J_1 \cos \varphi + J_2 \cos \psi + J_3 \sin \varphi \sin \psi + J_4 \cos \varphi \cos \psi \quad (2c)$$

where K<sub>0</sub>, K<sub>1</sub>, H<sub>0</sub>, H<sub>1</sub>, J<sub>1</sub>, J<sub>2</sub>, J<sub>3</sub>, and J<sub>4</sub> are functions of R, r<sub>g</sub>, r<sub>f</sub>, Θ, θ<sub>g</sub>, θ<sub>f</sub>, m<sub>O</sub> (mass of the oxygen atom), m<sub>C</sub> (mass of the two carbon atoms), m<sub>Mf</sub>, and m<sub>Mg</sub>. We do not report these functions explicitly,<sup>9,15</sup> but we show their values in Table 1, obtained by substituting the values of the geometrical parameters, in order to give an idea of the relative importance of each element. We noted that the most relevant contributions to the G elements are given not by the two heavy atoms M<sub>g</sub> and M<sub>f</sub>, but by the C<sub>1g</sub>, O<sub>1</sub>, and C<sub>2f</sub> atoms of the glycosidic linkage.<sup>16</sup> This also means that the conformational changes of the glycosidic linkage are brought about by the motions of C<sub>1g</sub>, O<sub>1</sub>, and C<sub>2f</sub>. Kinetically, the difference between the two units is mostly due to their different orientation defined by θ<sub>g</sub> and θ<sub>f</sub>. It is important for the study of the dynamical problem that the kinetic energy matrix not be diagonal and its elements nonlinearly depend on φ and ψ. This means that the two degrees of freedom are kinetically nonlinearly coupled.

The potential energy function that we used in Equation 1 is:

$$V(\varphi, \psi) = a(1 - \cos(\psi + 140^\circ)) + b(1 - \cos 3\psi) + c(1 - \cos(\varphi - 180^\circ)) \quad (3)$$

where a = 758 cm<sup>-1</sup>, b = 980 cm<sup>-1</sup>, and c = 4236 cm<sup>-1</sup>. V(φ,ψ) was constructed by adjusting to a simple functional dependence the adiabatic energy maps derived on the basis of MM by Tran and Brady<sup>3</sup> and Engelsen et al.<sup>4</sup> We noted that Tran and Brady used a coordinate  $\bar{\phi}$ , which is the dihedral

angle H<sub>1g</sub>-C<sub>1g</sub>-O-C<sub>2f</sub> and a coordinate  $\bar{\psi}$ , which is C<sub>1g</sub>-O-C<sub>2f</sub>-O<sub>5f</sub>. The relations to φ, and ψ of this work are:

$$\varphi = \bar{\varphi} + 180^\circ$$

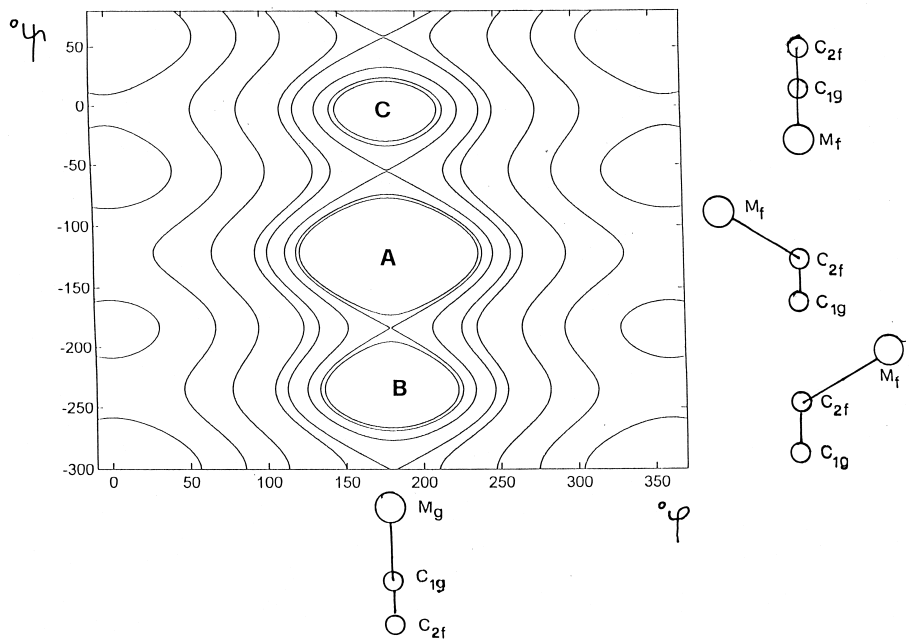
$$\psi = \bar{\psi} - 60^\circ$$

Equation 3 contains the principal findings of Tran and Brady<sup>3,4</sup>: three conformational minima A, B, and C, with energy differences and barriers as reported therein. To make the comparison easier, the contour map obtained for the potential function of Equation 3 is shown in Figure 3 and the values of the coordinates for the minima and saddles and energies thereof in wavenumber units and kcal/mole are given in Table 2. From the Ramachandran's map reported previously,<sup>3</sup> the lowest energy conformations are all contained in a channel with our angle φ between 90° and 270°. To keep a simple analytical function and to facilitate consideration of reactive dynamics, we considered the three minima A, B, and C aligned at φ = 180°. We noted that a difference of about ± 15° in φ was reported earlier<sup>3</sup> for point B and C, respectively. This alignment also has the great advantage of rendering ψ exactly the reaction coordinate. These simplifications notwithstanding, the contour map compares well with those reported earlier.<sup>3,4</sup> The major difference is for minimum C, for which discrepancies have been reported in the literature: its energy has been calculated as 2.7 kcal/mol<sup>3</sup> and 4.2 kcal/mol.<sup>4</sup> Finally, we observed that the contour maps derived<sup>3,4</sup> were explained as due in large part to a few intramolecular hydrogen bondings that are locking the glucose and fructose units into position A, B, or C. The resulting conformational energy is maintained in our model by the assumption of Equation 3, even though the description of intramolecular and/or intermolecular interactions is not possible here.

## RESULTS AND DISCUSSION.

The equations of motion for the two coordinates φ and ψ and their conjugated momenta p<sub>φ</sub> and p<sub>ψ</sub> were derived from the Hamiltonian of Equation (1). They were numerically integrated through a fourth-order Runge-Kutta routine of the SSP library,<sup>17</sup> with an integration step of 0.07 fs and with total integration times of up to a few nanoseconds, when necessary. To describe the dynamics of our system, the most important initial condition that we first define is the total energy E<sub>T</sub>, which is a constant of the motion. We then choose the other initial conditions in all the phase space compatible with this condition, always beginning each trajectory on the surface φ(t = 0) = φ<sup>0</sup> = 180°. Because the latter is the only minimum for V(φ,ψ) in the φ coordinate, every trajectory passes through it. We choose the initial value of the reactive coordinate and

**Figure 3.** Contour plot of the potential energy  $V(\phi, \psi)$  for sucrose employed in the calculations of the present work. The Newman projections of  $M_f C_{2f} O_1 C_{1g}$  are shown on the right, in correspondence with the three minima A, B, and C. The Newman projection for  $M_g C_{1g} O_1 C_{2f}$  common to all three minima is shown at the bottom.



conjugated momentum  $\psi(t=0) = \psi^\circ$  and  $p_\psi(t=0) = p_\psi^\circ$  in all phase space allowed, i.e., wherever  $H(\phi^\circ, \psi^\circ, p_\phi, p_\psi^\circ) = E_T$  admits solutions for  $p_\phi$  (called  $p_\phi^\circ$  hereafter). Because two roots for  $p_\phi^\circ$  are found, the one with higher value is always chosen.

We produce three kinds of plots for each initial condition:

- The time evolutions for the coordinates  $\phi(t)$  and  $\psi(t)$  and of some significant linear combinations thereof;
- The Lissajous maps, i.e., the trajectories in the configuration space  $(\phi, \psi)$ ;
- The Poincaré surface of sections (PSS), defined as the *loci* of the points in the plane  $(\psi, p_\psi)$  generated by each trajectory while crossing the hypersurface defined by the condition<sup>9,10</sup>:

$$\varphi = 180^\circ \text{ with } p_\varphi > -[g(180^\circ, \psi)/g(180^\circ)]p_\psi. \quad (4)$$

The last condition is necessary to make each point in the PSS correspond to just one dynamical state. Equation 4 reduces to the usual condition  $p_\phi > 0$ , in absence of cross kinetic terms in the Hamiltonian, as previously noted.<sup>9</sup> We note that the advan-

tage of considering these PSS maps is that, with  $\psi$ , being the reactive coordinate, the maps illustrate the reactive phase space.

## Nonreactive Dynamics

First, we describe the vibrational dynamics around the absolute minimum A for  $V(\phi, \psi)$  at different energies between  $E_A$  and  $E_{SAB}$  (Figure 4a). In Figure 4a, we show the PSS trajectories corresponding to  $E_T = E_A + 5\% E_{esc}$  ( $A \rightarrow B$ ),  $E_{esc}(A \rightarrow B) = E_{SAB} - E_A = 2110 \text{ cm}^{-1}$  being the energy barrier between conformations A and B. Each curve corresponds to an initial condition. At this low total energy, each initial condition generates a regular trajectory. In particular, we have two families of closed curves around two centers. The family in the upper part of the map occupies the region of positive  $p_\psi$  and invades part of the  $p_\psi < 0$  region; the family in the lower part is less extended and occupies the  $p_\psi < 0$  semiplane only partially. The two centers are fixed points of order one: the mapping, i.e., the PSS, gives always exactly the same one point at each intersection (if it gives a set of n fixed points every n iterations, one speaks of fixed points of order n).<sup>10</sup> The center of the lower family of curves in the PSS corresponds to the *antisymmetric normal mode*. As shown in Figure 4b (right), during time evolution.  $\phi$  and  $\psi$  are opposite in phase and the amplitude of the oscillation in  $\psi$  is twice that of  $\phi$ . This mode is characterized by just one frequency  $\omega_A$  and gives rise to a straight line in the Lissajous map with a slope related to the ratio of the two amplitudes. The fixed point in the upper part of the PSS corresponds to a *symmetric normal mode* as it turns out from the phase relation observed in the temporal evolution of the two coordinates  $\phi$  and  $\psi$ , presented in Figure 4b(left). This mode is dominated by an oscillation in the  $\phi$  coordinate, whose amplitude is three times that of  $\psi$ . This second coordinate oscillates with two frequencies: the principal one,  $\omega_S$ , coincides with that of the  $\phi$  coordinate; the other,  $\omega'_S$ , is exactly two times  $\omega_S$ . This fact reveals itself in the Lissajous map which is slightly curved

**Table 2.** Values for the  $\varphi$  and  $\psi$  coordinates and of the potential energy at the three minima A, B, and C and at the three saddles  $S_{AB}$ ,  $S_{AC}$ , and  $S_{BC}$  for the potential function  $V(\varphi, \psi)$  given by Equation 3

	$\varphi$	$\psi$	$E (\text{cm}^{-1})$	$E (\text{kcal/mol})$
A	$180^\circ$	$-122^\circ$	42.5	0.121
B	$180^\circ$	$-235^\circ$	858.	2.45
C	$180^\circ$	$-3.5^\circ$	1325.	3.78
$S_{AB}$	$180^\circ$	$-182^\circ$	2152.	6.15
$S_{AC}$	$180^\circ$	$-55^\circ$	2618.	7.48
$S_{BC}$	$180^\circ$	$58.5^\circ$	3433.	9.8

See also Figure 3.

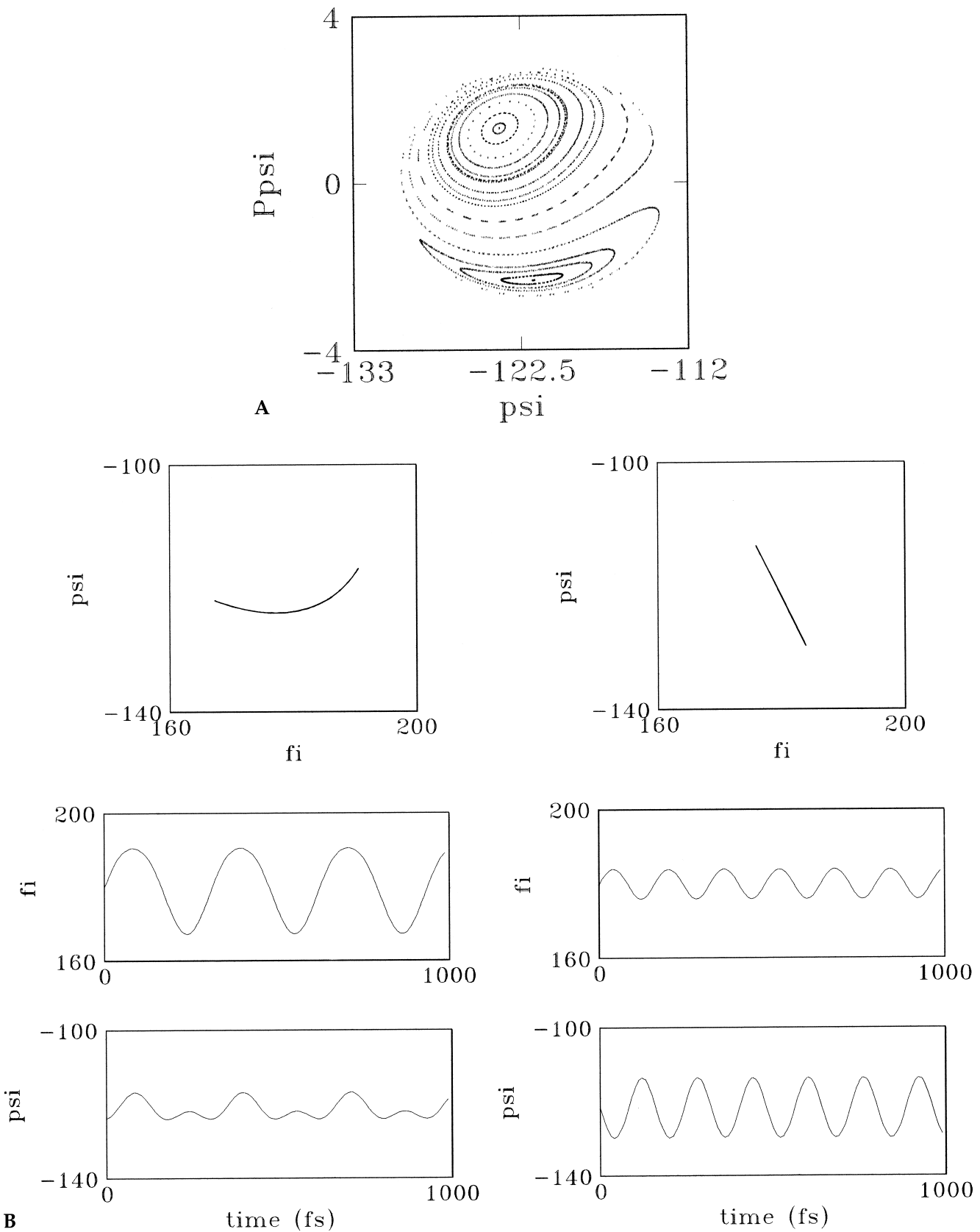


Figure 4. (a) Poincaré surfaces of section in the  $(\psi, p_\psi)$  plane for energy  $E_T = 148 \text{ cm}^{-1} = E_A + 5\% E_{esc}$  ( $A \rightarrow B$ ) in the vicinity of conformational minimum A of Figure 3. Units are degrees for the abscissa axis and (a.m.u.  $\cdot \text{\AA}^2 \cdot \text{degrees} \cdot \text{fs}^{-1}$ ) for the ordinate axis. (b) Lissajous maps and time evolutions for the symmetric (left) and antisymmetric (right) fixed points.

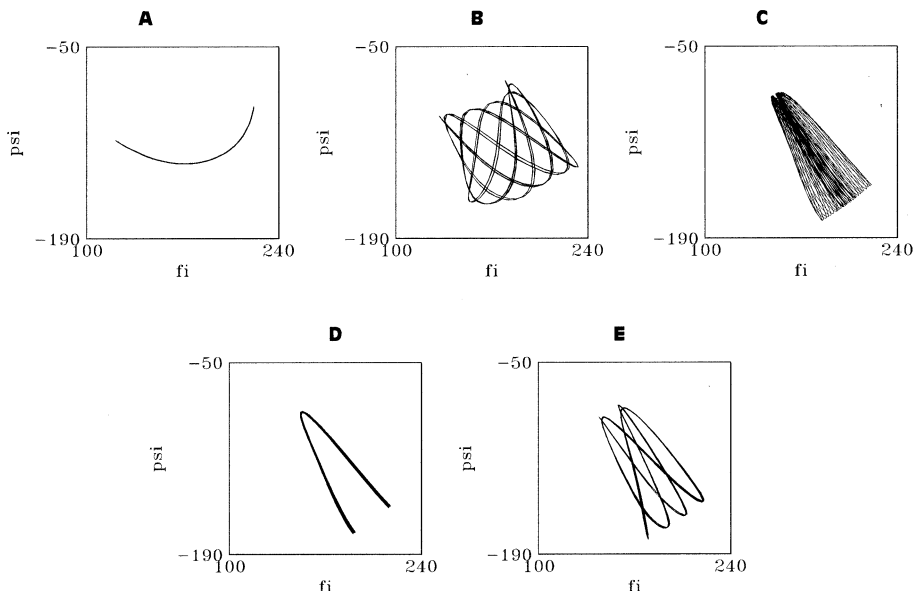


Figure 5. Lissajous maps of the (A) symmetrical fixed point trajectory; (B) the 7:12 resonant trajectory in the border region between symmetrical and antisymmetric modes; (C) a chaotic trajectory close to the antisymmetric fixed point; (D) the 2:1 resonant trajectory in the antisymmetrical modes region; and (E) the 4:7 resonant trajectory (see text).

and is topologically equivalent to that of a 2:1 resonance<sup>18</sup>; the component in the  $\omega_s'$  frequency being clearly very small. Finally, we observe that the frequency  $\omega_s'$  almost coincides with the frequency  $\omega_A$  of the antisymmetric mode noted above. As expected for low energies, the frequency and amplitude of the oscillations are unrelated, with the frequency being just the curvature of the potential. The  $\psi$  coordinate has a higher frequency than the  $\phi$  coordinate, because there are three minima in  $360^\circ$  instead of one. The presence of either one or two frequency components in one mode can be described as follows. In the case of antisymmetric modes, the  $\psi$  oscillations force oscillations in  $\phi$ , so that they behave exactly as the usual normal modes of the harmonic vibrational systems. In contrast, when the less tight angle  $\phi$  is mainly oscillating, as in the symmetric mode, it forces the  $\psi$  component but does not completely lock it, because the  $\phi$ -natural frequency is smaller than the  $\psi$ -natural frequency. The trajectories surrounding the two fixed points just described correspond to quasiperiodic modes. They resemble the two periodic modes in frequencies and relative amplitudes of the coordinates, but two frequencies are present in each mode that are not multiples of one another. As long as the ratio of the two frequencies is irrational, KAM theory is valid, and thus each trajectory moves on a torus, giving rise to regular curves in the PSS and chaos does not appear.<sup>10-12</sup> We expect that, by increasing the total energy, frequencies vary and start to depend on amplitudes due to anharmonicity,<sup>10</sup> giving rise to new resonances and new families of curves. Finally, tori are destroyed. In our system, the situation described for  $E_T = E_A + 5\%E_{esc}$  ( $A \rightarrow B$ ) does not qualitatively change with increasing energy except for very high energy values. Until  $E_T \approx E_A + 80\%E_{esc}$  ( $A \rightarrow B$ ), there are just two families of regular curves and practically the same observations can be made about amplitude ratios and frequencies of the fixed points. With increasing energy, the frequencies decrease, but the antisymmetric mode frequency  $\omega_A$  becomes significantly lower, while the characteristic frequencies of the symmetric mode,  $\omega_s$  and  $\omega_s'$ , change slightly because  $V(\phi, \psi)$  changes slightly in  $\phi$  for  $E_T \approx E_A + 80\%E_{esc}$  ( $A \rightarrow B$ ).

At  $E_T = E_A + 99\%E_{esc}$  ( $A \rightarrow B$ ), the situation dramatically

changes, as apparent from Color Plate 1a in which each color corresponds to an initial condition (occasionally, we may see trajectories with the same color because of the limited availability in the number of colors). The family of regular curves around the symmetric fixed point (the Lissajous map shown in Figure 5a) remains practically unaltered, and percentagewise occupies the same phase space portion as at lower energies, invading the region  $p_\psi < 0$ . Just one island chain can be observed inside this family, about the equatorial line  $p_\psi = 0$ , corresponding to a 7:12 resonance. The frequency ratio of a resonance can be checked from the time evolution plots of the coordinates  $\phi$  and  $\psi$ , or, in the case of higher order resonances, from the time evolution of appropriate linear combinations of  $\phi$  and  $\psi$ . When looking at the plots of  $(3\phi + \psi)$  and  $(\phi - 3\psi)$  vs time, we saw seven oscillations in the first combination for each 12 oscillations of the second one. The Lissajous map of Figure 5b describes adequately the resonance, bearing in mind that an n:m resonance is characterized by n oscillations in one direction and m oscillations in the other direction.<sup>18</sup> The family of regular curves corresponding to  $p_\psi < 0$  is instead destroyed. The antisymmetric fixed point becomes unstable and the tangled trajectories that are generated<sup>10-12</sup> give rise to the chaotic region colored in purple. At the same time, two stable fixed points are originated on the two sides (fixed point of order two), a situation contemplated by the Poincaré-Birkhoff theorem<sup>10,18,19</sup> and that can be described as a pitchfork bifurcation. The Lissajous map of the chaotic trajectory is qualitatively reminiscent of the map of the corresponding stable fixed point at low energy (Figure 5c and Figure 4b left). The Lissajous map of the two stable new fixed points is typical of a 2:1 resonance, as seen in Figure 5d. Apart from the limited two regions of regular curves surrounding these two new centers, the region  $p_\psi < 0$  is chaotic and is a typical example of how chaos makes its appearance just after the destruction of tori. It can be observed that trajectories do not scatter uniformly in all the phase space not occupied by regular KAM curves. On the one hand, KAM curves around the new stable fixed points prevent chaos from invading all phase space.<sup>10-12</sup> On the other hand, the stable and unstable manifold of hyperbolic fixed

points, according to the Poincaré-Birkhoff theorem, constitute partial separatrices and keep the chaotic trajectory trapped in the tangle, until it enters some structures of the separatrix described in the literature as “turnstiles” by MacKay et al.<sup>19</sup> This is the situation shown in Color Plate 1. The diffusion of chaos in the direction orthogonal to the destructed tori is nearly forbidden. Considering Color Plate 2, which is an enlarged portion of Color Plate 1, it is evident that many island chains prevent diffusion from the unstable purple antisymmetric region (close to  $\psi = -120^\circ$ ) to the green chaotic region, and to the red one, bordering with the stable symmetric region. About the resonances that can be observed (on this scale), we give as an example the Lissajous map (Figure 5e) of seven black islands that result in a 4:7 resonance. The theory of transport in chaotic Hamiltonian systems first proposed<sup>19</sup> using the standard map as prototype must be borne in mind when considering reactive dynamics.<sup>13,20,21</sup> In particular, the importance of resonances as structures underlying chaos and preventing it from being uniform have been recognized for a long time.<sup>10-12</sup>

Let us now briefly describe the dynamics about the two conformational minima B and C (Figure 3). In both cases, at very low energy the situation is practically identical to that of minimum A. Symmetric modes exhibit a prevalence in the  $\phi$  coordinate, and antisymmetric modes exhibit high variations of angle  $\psi$ .

At  $E_T = E_B + 99\%E_{esc}$  ( $B \rightarrow A$ ) in B, with  $E_{esc}$  ( $B \rightarrow A$ ) =  $E_{SAB} - E_B = 1294 \text{ cm}^{-1}$ , both the symmetric and the antisymmetric fixed points remain stable, as shown in Color Plate 3a. In the region  $p_\psi > 0$ , a 3:5 resonance is evident. Moreover, as for minimum A, the region occupied by chaotic trajectories, which are of the kind eventually leading to interconversion at higher energy, is the one with  $p_\psi < 0$ , corresponding to antisymmetric type modes. Consequently, the resonances in this region can be important when examining reactivity; one can easily distinguish a 3:5 resonance in the five black points in the chaotic region just outside the regular quasiperiodic antisymmetric modes and a 5:8 resonance.

At  $E_T = E_C + 99\%E_{esc}$  ( $C \rightarrow A$ ) in conformational minimum C, with  $E_{esc}$  ( $C \rightarrow A$ ) =  $E_{SAC} - E_C = 1293 \text{ cm}^{-1}$ , the same analysis can be performed. We show the corresponding PSS in Color Plate 3b. In this case, chaos is still absent on the scale of observation. More importantly, the largest changes as function of total energy in this conformation do not involve antisymmetric modes but rather the symmetric ones. Unlike what was been observed for minima A and B, with increasing energy  $E_T$  the symmetric fixed point becomes unstable, and two stable fixed points are observed, both of them are a 1:4 resonance, with two Lissajous maps that are approximately mirror images of one another. The only hint of chaos observed in this map is that of the separatrix between the two new 1:4 families of regular curves.

## Reactive Dynamics

We will discuss here the conformational isomerization reaction from minimum A to minimum B or vice versa. The dynamics from C to B and/or to A or vice versa will not be discussed due to the peculiar differences noted earlier for the vibrational dynamics in conformation C with respect to both A and B (which look similar). The conclusions reported may not necessarily apply for the reactions  $C \leftrightarrow A$ ,  $C \leftrightarrow B$ , and  $A \leftrightarrow C \leftrightarrow B$ , but the methods reported are applicable. In Color Plate 4 we

present the PSS relative to  $E_T = 2258 \text{ cm}^{-1} = E_B + 105\%E_{esc}$  ( $B \rightarrow A$ ). The region with  $p_\psi > 0$  is mostly occupied by regular KAM curves, which cannot sustain any reaction.

In the basin of the conformational minimum A, in addition to the 7:12 resonance observed at  $E_T = E_A + 99\%E_{esc}$  ( $A \rightarrow B$ ) at the border of the regular symmetric modes region (shown in blue), a 5:9 resonance appears, generating the five black fixed points halfway between the 7:12 resonance and the symmetric fixed point. In the equatorial region  $p_\psi = 0$ , a 3:5 resonance is observed, which is surrounded by chaos.<sup>22</sup>

In the basin of the conformational minimum B, in addition to the 3:5 resonance observed in Color Plate 3a for energy  $E_T = E_B + 99\%E_{esc}$  ( $B \rightarrow A$ ), a 4:7 resonance is observed, halfway between the 3:5 resonance and the symmetric fixed point.

The chaotic behavior observed for  $p_\psi < 0$  at  $E_T = E_A + 99\%E_{esc}$  ( $A \rightarrow B$ ) in both potential wells now becomes well extended in phase space. The chaotic region looks uniform; it is difficult to distinguish partial barriers to diffusion inside chaos that are evident in Color Plate 2 at  $E_T = E_A + 99\%E_{esc}$  ( $A \rightarrow B$ ). The chaotic region present in Color Plate 4 was studied by examining six initial conditions starting from there, four of which were integrated for 50 ps, one for 1 ns and one for 3 ns. Nearly all of the portion of phase space occupied by chaos is covered by each one of them, except for the thin layer around the regular curves of conformation B and for the “separatrix” between the regular curves and the resonance 3:5 mentioned earlier for conformational minimum A. The two latter regions are difficult for trajectories to enter and to exit, especially the second one. From the point of view of conformational reactivity, they behave as if they were separated from the rest of chaos. Considering interconversion between conformations A and B, we want to show further numerical data that may allow calculation of the probability of interconversion and that describe the characteristics of the reacting trajectories. It is obvious that every initial condition that is picked up in the regular part of phase space, or in any case in a region delimited by a KAM curve, will never give rise to reaction, i.e., will never cross the line  $\psi = -182^\circ$  in Color Plate 4. On the contrary, every trajectory starting in any point of the chaotic region that extends in both wells A and B will definitely react and will back-react at a successive time. As already noted in many dynamical systems, the probability of reaction is not uniform in the entire chaotic region, contrary to the usual hypothesis of RRKM theory.<sup>23</sup> A first interesting proof that chaos is nonstructureless in the present system can be achieved by a numerical experiment analogous to that done by Marston and De Leon in studying the interaction of ring puckering and PH-inversion in phospholene.<sup>13</sup> In Color Plate 5, we show a PSS map that was built by reporting not all the intersections of the phase space trajectories with the plane  $\phi = 180^\circ$  (see Equation 4), but only those that are immediately prior to the crossing of the barrier  $S_{AB}$  or immediately after the crossing of the barrier. The former are marked in blue; the latter are marked in red. These points are not scattered over the entire chaotic region, as one would expect in uniform chaos, neither are they concentrated close to the barrier, as it would occur in slow and partially ordered diffusion. In fact, they fill up few well-defined regions that are de facto “doors” to exit basins A or B or to enter them. These structures have been called “reactive islands” (RIS),<sup>13</sup> where they were studied in general by analyzing the properties of the unstable periodic orbits, that is, they were correlated to the successive PSS mappings of the

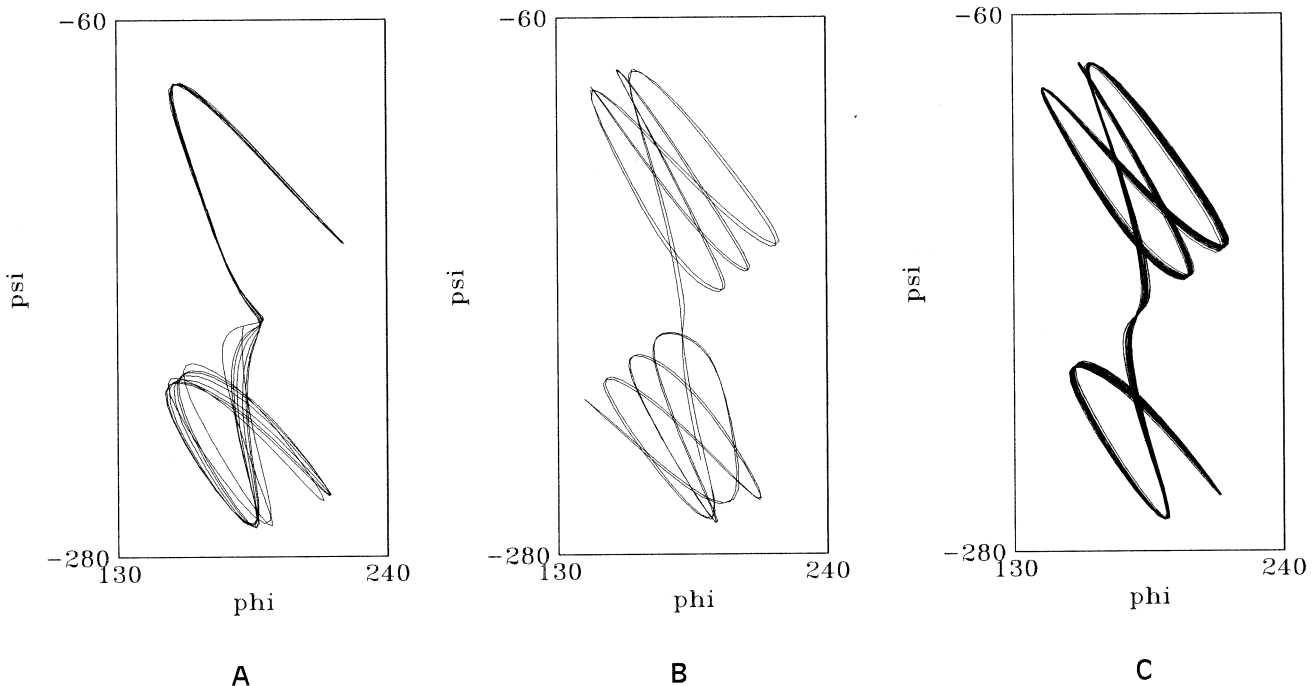


*Figure 6.* Lissajous maps for selected trajectories at energy  $E_T = 2217 \text{ cm}^{-1} = E_B + 105\% E_{\text{esc}}$  ( $B \rightarrow A$ ) in the vicinity of both conformational minima A and B of Figure 3 (see Color Plates 4 and 5) for (A) the 1:2 resonant trajectory in A plus the 2:3 resonant trajectory in B; (B) the 4:7 resonant trajectory in A plus the 5:8 resonant trajectory in B; and (C) the composite 3:5 in A and 2:3 in B resonant trajectory.

stable and unstable manifolds emanating from hyperbolic fixed points. Repeating such a detailed analysis for the present model is beyond the scope of our work. We drew our considerations by looking at the structures presented in Color Plate 5. First, it is obvious that the exit blue area must be equal to the enter red area. These regions are densely filled and are obtained independently from the initial conditions used to generate the trajectories. They seem to be contained by smooth curves,<sup>13</sup> and their area is independent of the total integration time and the number of considered trajectories. Longer integration times or larger numbers of initial conditions allow the trajectories to better fill these regions. The meaningfulness of these well-delimited structures in the chaotic region of phase space is that every reactive trajectory (even starting from other parts of the phase space) must first go through a blue region before reaction and ends up in a red region. Reactive islands contain all the reactive phase space points (in blue) or the just reacted ones (in red) and only them. If we name  $\alpha, \beta$  (in B)  $\gamma, \delta$  (in A) the four exit reactive regions and  $\alpha', \beta'$  (in A),  $\gamma', \delta'$  (in B) the corresponding four enter regions, we have verified that every initial condition in  $\alpha$  generates a trajectory entering conformer A either in  $\alpha'$  or in  $\beta'$  (the latter occurs for points in  $\alpha$  at low  $p_\psi$  value); trajectories through points in  $\beta$  end up in region  $\alpha'$  with low  $p_\psi$  values; and every trajectory through  $\gamma$  or  $\delta$  in conformer A reacts to B in the regions  $\gamma'$  or  $\delta'$ , respectively.

“Reactive islands” are present just above the barrier. For example, we were able to locate them at  $E_T = E_B + 101\% E_{\text{esc}}$  ( $B \rightarrow A$ ). They increase in size with increasing total energy  $E_T$ . At  $E_T = E_B + 110\% E_{\text{esc}}$  ( $B \rightarrow A$ ),  $\alpha'$  and  $\delta$  in A and  $\alpha$  and  $\delta'$  in B superimpose, which increases reactivity more and more.

Finally, we wish to comment on selected examples of reac-

tive trajectories. We chose them from the cases at  $E_T = E_B + 105\% E_{\text{esc}}$  ( $B \rightarrow A$ ), but an analogous analysis can be carried out at other energy values. We find that any given reactive trajectory stays in one of the conformers for a long time only if it happens to visit one of the two phase space regions, i.e., the border of chaos near the regular modes in minimum B (we recorded two examples of this for 25 ps and 60 ps) and the fully chaotic region between the regular symmetric modes and the 3:5 resonance in minimum A (we recorded one trajectory trapped in that region for 500 ps). In the rest of the chaotic region, the time of permanence of trajectories in each well is quite short. All examined chaotic trajectories, in short time intervals (on the order of picoseconds), behave like the resonances that are embedded in chaos, as can be documented by the Lissajous maps generated for time intervals large enough to let the trajectory visit the phase space region near the resonance. In this case, the trajectory remains in the well A (or B) for the time needed to complete the m:n resonance or a multiple of it. Hopping of the trajectory from one resonance to another inside the same well is a slow, highly unlikely process. The resonances that we recognized are those described earlier, because they survive from  $E_T = E_B + 99\% E_{\text{esc}}$  ( $B \rightarrow A$ ) and  $E_T = E_A + 99\% E_{\text{esc}}$  ( $A \rightarrow B$ ). In particular, we found reactive trajectories following closely the 1:2 and the 4:7 resonances in region A, and the 5:8 resonance in region B. The reaction between A and B is guided so efficiently by all the resonances just mentioned, because all their Lissajous maps were observed to possess one turning point at the saddle, such that two of them, one in A and one in B, can join smoothly. This is illustrated by the two Lissajous maps of Figure 6A, which shows the 1:2 resonance of conformer A together with the 2:3

resonance of conformer B (discussed later), and of Figure 6B, which shows the 4:7 resonance of conformer A and the 5:8 resonance of conformer B. In addition, another interesting resonance embedded in chaos appears at this energy, described by one set of fixed points extending partly in A and partly in B. We were able to catch a chaotic trajectory quite close to this resonance that showed up as an ensemble of black fat dots in Color Plate 4, because the trajectory passes close to the resonance many times. Five of the dots are in region A, three are in region B, and one is very close to the saddle  $\psi = -182^\circ$ , with  $p_\psi > 0$ . From the Lissajous map shown in Figure 6C, this resonance can be classified as 2:3 in B and 3:5 in A. Again it is observed that the two parts of the Lissajous map in the two wells go smoothly into one another.

Finally, if we compare the PSS intersections of the chaotic trajectories close to resonances with the reactive RIS regions in Color Plate 5, we see that all these resonances have one point in one of the escape regions (blue) and one point in one of the entering regions (red). Referring to the examples cited earlier, we see that the two PSS points of the 1:2 resonance are one in  $\alpha'$  and one is in  $\delta$ . The PSS points of the complex 2:3 resonance in B/3:5 resonance in A are distributed as follows: one point is observed in  $\delta'$  and one in  $\beta$  in the B basin, one point is observed in  $\alpha'$  and one in  $\gamma$  in the A basin.

We can state that the conformational isomerization reaction A→B in sucrose is guided by all those resonances in phase space that occupy a strip containing the reactive RIS structures. All observations expounded about this highly simplified model indicate that the conformational interconversion from A to B and vice versa occurs through modes in which the two torsions have an antisymmetric phase relation, with a prevalence of the oscillations in the  $\psi$  coordinate. Symmetric vibrations do not lead to interconversion. We recall that, in our dynamic study, we do not define a value for the temperature as in standard MD studies,<sup>3–8</sup> but a value for the total energy, which is distributed between two degrees of freedom only, with the effect of all the other degrees being included in our model ad hoc into an effective potential. The main assumption of the present model, i.e., that just the two degrees of freedom  $\phi$  and  $\psi$  are needed to describe isomerization of the glycosidic linkage, intrinsically enhances the reactivity rate, because it is not necessary to wait to have enough energy on the reaction coordinate. By RRKM arguments, the time for unimolecular conformational isomerization is longer when the number of degrees of freedom coupled to the reaction coordinate  $\psi$  is larger.<sup>23</sup> For this reason, we obtained reaction and back-reaction in very short times (a few picoseconds) when encountering reactive resonances. The probability of this occurring is proportional to the area of the “reactive islands” and not just to the chaotic area. There are regions in chaos, not separated by regular trajectories from the saddle, but nonetheless nearly as inefficacious in reacting. In practice, diffusion from these regions to reactive regions is very slow in comparison to the simple reaction time. Last, but not least, in evaluating the reaction probability, we note that a large part of the accessible phase space is occupied by multiperiodic trajectories [approximately 50% for  $E_T = E_B + 105\% E_{esc}$  (B→A)]. These trajectories are strictly nonreactive and survive for an infinite time in the present model. In standard MD calculations, the molecule exits from such trajectories by fluctuat-

ing interactions that have been neglected in our model; in any case, this would increase the time for reaction.

## CONCLUSIONS

In this paper we studied the dynamics of the dihedral angles  $\phi$  and  $\psi$  about the glycosidic linkage in sucrose, by applying a method that we had previously developed and applied to the study of  $\beta,\beta$ -trehalose.<sup>9</sup> The method is based on the study of the phase space structure associated with four-dimensional space  $(\phi, \psi, p_\phi, p_\psi)$ . The study consisted of the construction of Poincaré surfaces of section, Lissajous maps, and temporal evolution plots of the two dihedral angles. Due to the quite drastic difference in the behavior of the angles  $\phi$  and  $\psi$ , as described in the Ramachandran's plots,<sup>3,4</sup> such that  $\psi$  plays the role of reacting coordinate, a marked difference from the dynamic behavior is noted in sucrose from trehalose, where the  $\phi, \phi'$  dihedral angles are equivalent by symmetry. With increasing energy, the antisymmetric mode in sucrose becomes unstable, whereas the symmetric mode remains stable. In trehalose, the two normal modes were found to be equally stable or unstable, and a stochastic layer was observed to grow quickly between them.<sup>9</sup> In sucrose, the latter layer instead grows in the portion of phase space previously occupied by antisymmetric normal modes. By our method, the central role of resonances is recognized not only in defining the phase space structure at all energies, but also as underlying the possible mechanisms of conformational isomerization. Characterization of the resonances that are present in chaos also was discussed in a different context by Losada et al.<sup>24</sup> In this system, we recognized resonances that act as barriers to diffusion through their partial separatrices<sup>19–21</sup> so as to hinder the reaction, and other resonances, deeply embedded in the chaotic portion of the phase space, that instead guide the reaction. The latter ones were located in the most reactive part of the phase space, namely the reactive islands (RIS) found by Marston and De Leon<sup>13</sup>.

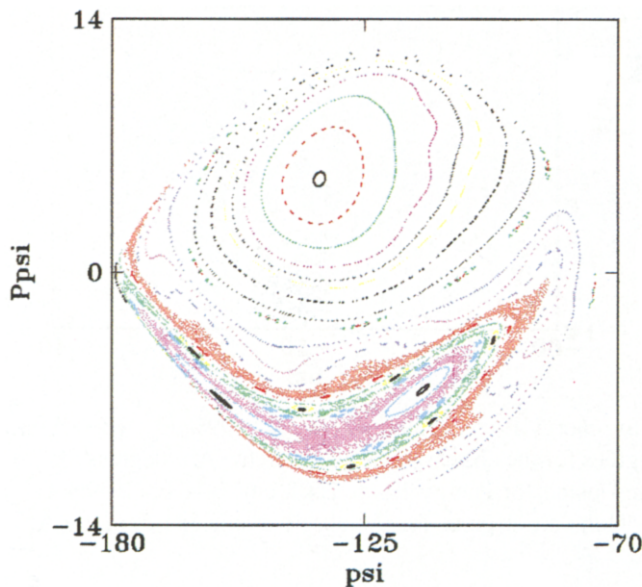
Even though it is still premature to obtain reaction times or unimolecular reaction rate constants from our method, a qualitative step forward has been made. The trapping of trajectories in the conformational minima A or B (Figure 3) that were observed previously<sup>3,4</sup> is rationalized here in terms of (i) the survival of a large fraction of regular trajectories even at energies higher than the interconversion barrier and (ii) the existence of portions of the chaotic region, trapping reactive trajectories in basins A or B. In this case, a long diffusion time toward “reactive islands” inside each conformer is the rate-determining step of the isomerization reaction.

## REFERENCES

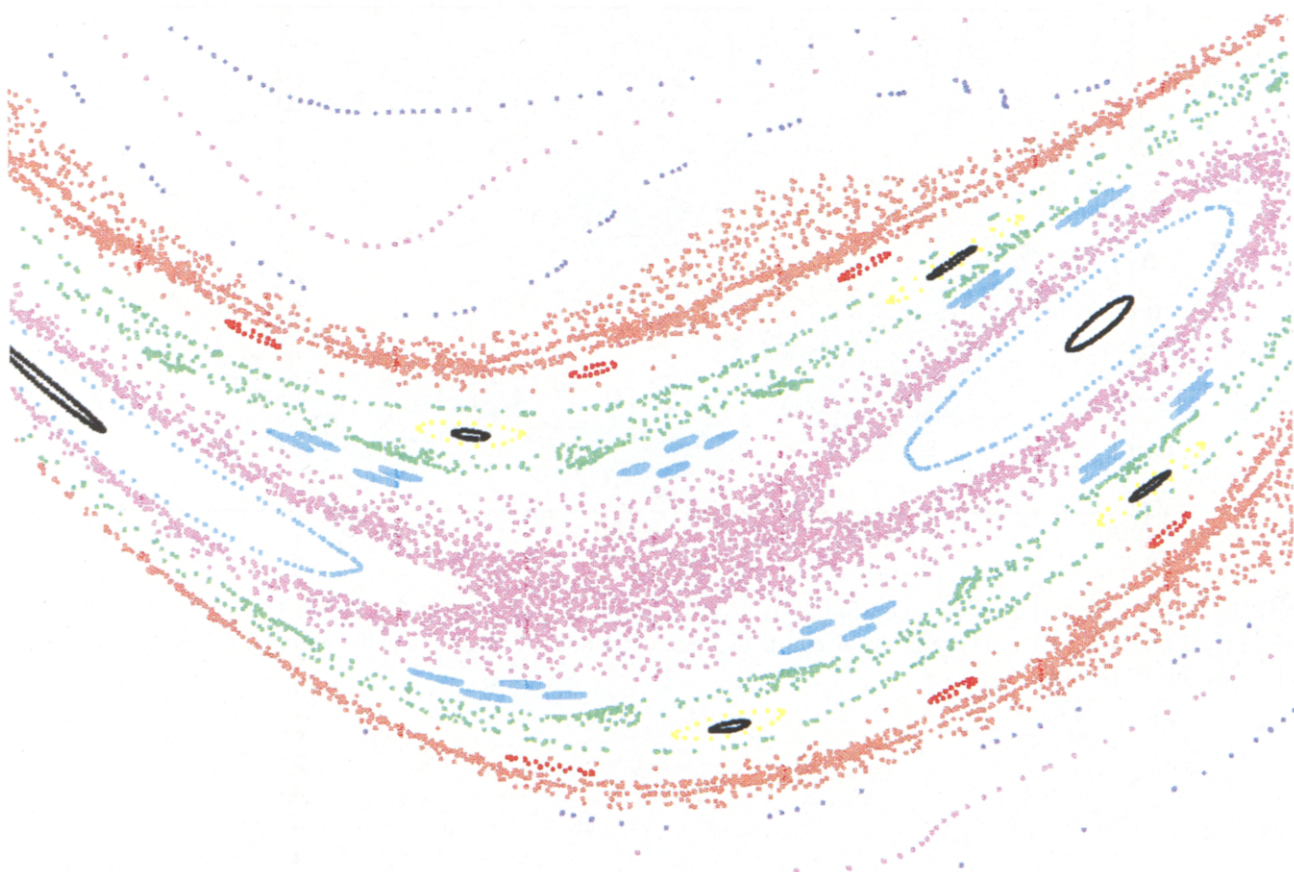
- 1 Karplus, M., and Petsko, G.A. Molecular dynamics simulations in biology. *Nature* 1990, **347**, 631–639
- 2 Brady, J.W. Molecular simulations of  $\alpha,\alpha$ -glucose. *J. Am. Chem. Soc.* 1986, **108**, 8153–8160
- 3 (a) Tran, V.H., and Brady, J.W. Disaccharide conformational flexibility. I. An adiabatic potential energy map for sucrose. *Biopolymers* 1990, **29**, 961–976. (b) Tran, V.H., and Brady, J.W. Disaccharide conformational flexibility. II. Molecular dynamics simulations of sucrose. *Biopolymers* 1990, **29**, 977–997
- 4 Engelsen, S.B., Hervé du Penhoat, C., and Pérez, S.

- Molecular relaxations of sucrose in aqueous solution: how a nanosecond molecular dynamics simulation helps to reconcile NMR data. *J. Phys. Chem.* 1995, **99**, 13334–13351
- 5 Donnamaria, M.C., Howard, E.J., and Grigera, J.R. Interactions of water with  $\alpha,\alpha$ -trehalose in solution: Molecular dynamics simulations in water. *J. Chem. Soc. Faraday Trans.* 1994, **90**, 2731–2735
- 6 Billeter, S.R., and van Gunsteren, W.F. A modular approach molecular dynamics/quantum dynamics program for non-adiabatic proton transfer in solution. *Comp. Phys. Commun.* 1997, **107**, 61–91
- 7 Molteni, C., and Parrinello, M. Glucose in aqueous solution by first principles molecular dynamics. *J. Am. Chem. Soc.* 1998, **120**, 2168–2171
- 8 Bonanno, G., Noto, R., and Fornili, S.L. Water interactions with  $\alpha,\alpha$ -trehalose: Molecular dynamics simulations. *J. Chem. Soc. Faraday Trans.* 1998, **94**, 2755–2762
- 9 Abbate, S., Biancardi, L., Longhi, G., and Conti, G. Study of the phase space structure for a two-degrees of freedom model of a symmetric glycosidic linkage. *Carbohydr. Res.* 1997, **300**, 59–62
- 10 Lichtenberg, A.J., and Lieberman, A.M. Regular and chaotic dynamics, 2nd edition. Springer Verlag, New York, 1992
- 11 Tabor, M. Chaos and integrability in nonlinear dynamics. John Wiley, New York, 1979
- 12 Berry, M.V. Regular and irregular motions. *AIP Conf. Proc.* 1978, **46**, 27
- 13 (a) De Leon, N., and Marston, C.C. Order in chaos and the dynamics and kinetics of unimolecular conformational isomerization. *J. Chem. Phys.* 1989, **91**, 3405–3425. (b) Marston, C.C., and De Leon, N. Reactive islands as essential mediators of unimolecular isomerization: A dynamical study of 3-phospholene. *J. Chem. Phys.* 1989, **91**, 3392–3404
- 14 (a) Brown, G.M., and Levy, H.A. Further refinement of the structure of sucrose based on neutron-diffraction data. *Acta Cryst.* 1973, **B29**, 790–797. (b) Hanson, J.C., Sieker, L.C., and Jensen, L.H. Sucrose: X-ray refinement and comparison with neutron refinement. *Acta Cryst.* 1973, **B29**, 797–808
- 15 Decius, J.C. A tabulation of general formulas for inverse kinetic energy matrix elements in acyclic molecules. *J. Chem. Phys.* 1954, **16**, 1025–1033
- 16 Wilson, E.B. Jr., Decius, J.C., and Cross, P.C. *Molecular vibrations*. McGraw-Hill, New York, 1955
- 17 SSP Scientific and Statistical Package, IBM Corporation, Armonk, NY
- 18 Alonso, M., and Finn, E.S. *Fundamental university physics*. Addison-Wesley, London, 1969
- 19 (a) MacKay, R.S., Meiss, J.D., and Percival, I.C.. Transport in Hamiltonian systems. *Physica* 1984, **13D**, 55–81. (b) MacKay, R.S., Meiss, J.D., and Percival, I.C. Resonances in area-preserving maps. *Physica* 1987, **27D**, 1–20. (c) Bensimon, D., and Kadanoff, L. Extended chaos and disappearance of KAM trajectories. *Physica* 1984, **13D**, 82–89
- 20 Gray, S.K., Rice, S.A., and Davis, M.J. Bottlenecks to unimolecular reactions and an alternative form for classical RRKM theory. *J. Phys. Chem.* 1986, **90**, 3470–3482
- 21 Gray, S.K., and Rice, S.A. Phase space bottlenecks and statistical theories of isomerization reactions. *J. Chem. Phys.* 1987, **86**, 2021–2035
- 22 The fixed points observed in the map of Color Plate 4 are four, because that PSS map is not built using the correct combinations of  $\phi$  and  $\psi$  to give the resonance. This is also the reason for their distortion with respect to the “circles” of regular curves.
- 23 Gilbert, R.G., and Smith, S.C. *Theory of unimolecular and recombination reactions*. Blackwell, Oxford, 1990
- 24 Losada, J.C., Estebaranz, J.M., Benito, R.M., and Bordonio, F. Local frequency analysis and the structure of classical phase space of the LiNC/LiCN molecular system. *J. Chem. Phys.* 1998, **108**, 63–71

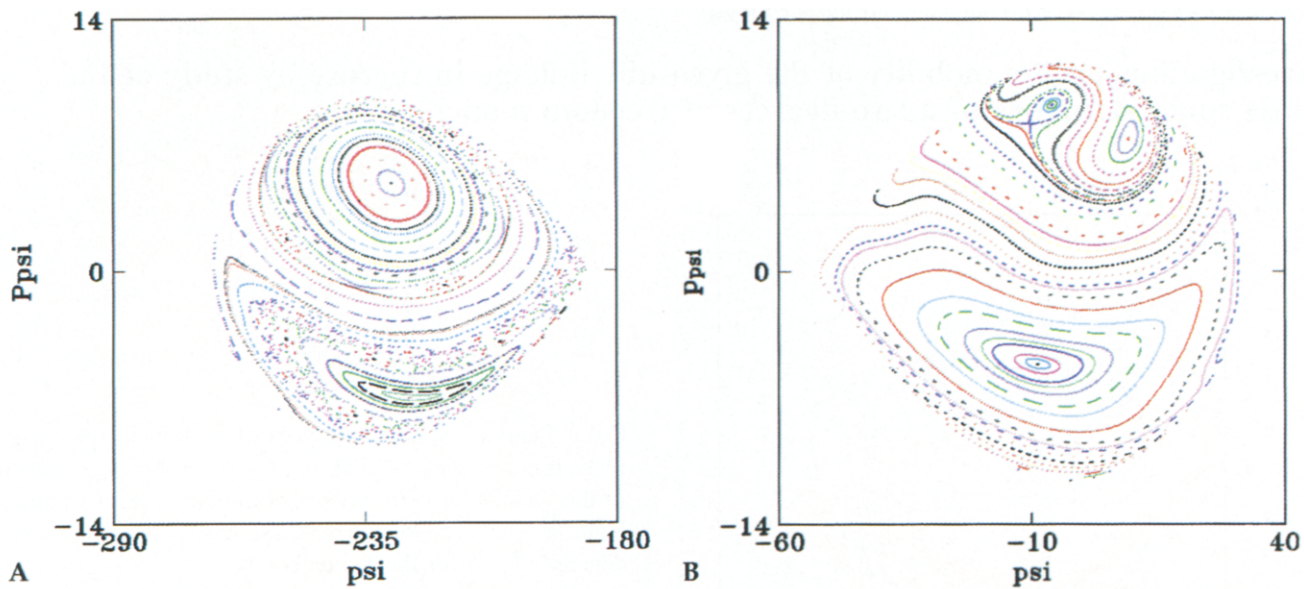
## Investigations on the mobility of the glycosidic linkage in sucrose by study of the phase space structure of a two-degrees of freedom model



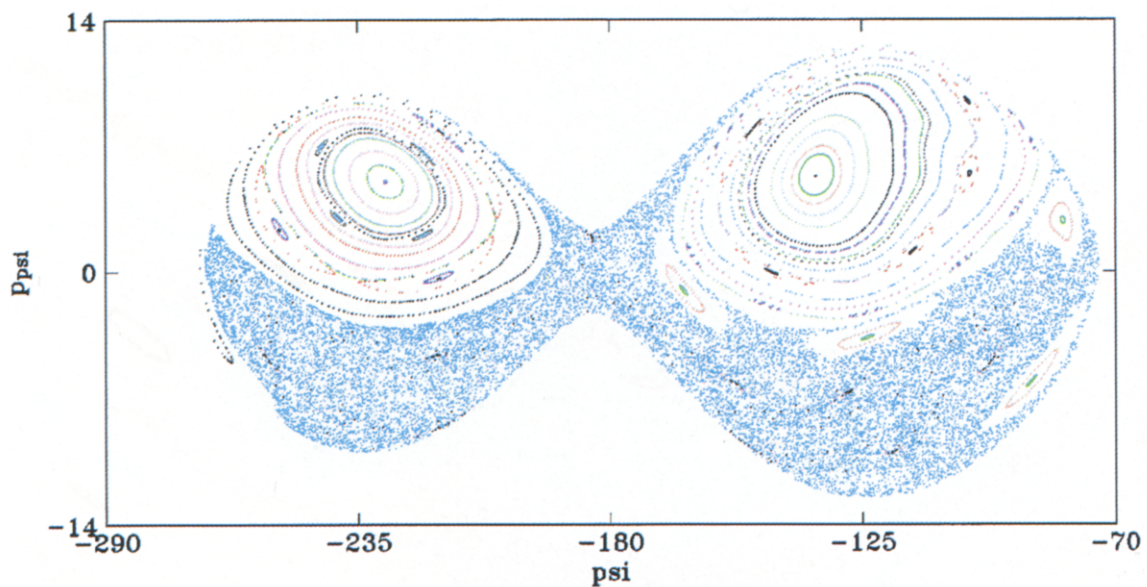
Color Plate 1. Poincaré surfaces of section in the  $(\psi, p_\psi)$  plane for energy  $E_T = 2131 \text{ cm}^{-1} = E_A + 99\% E_{\text{esc}} (A \rightarrow B)$  in the vicinity of conformational minimum A of Figure 3. Units are degrees for the abscissa axis and (a.m.u.  $\cdot \text{\AA}^2 \cdot \text{degrees} \cdot \text{fs}^{-1}$ ) for the ordinate axis.



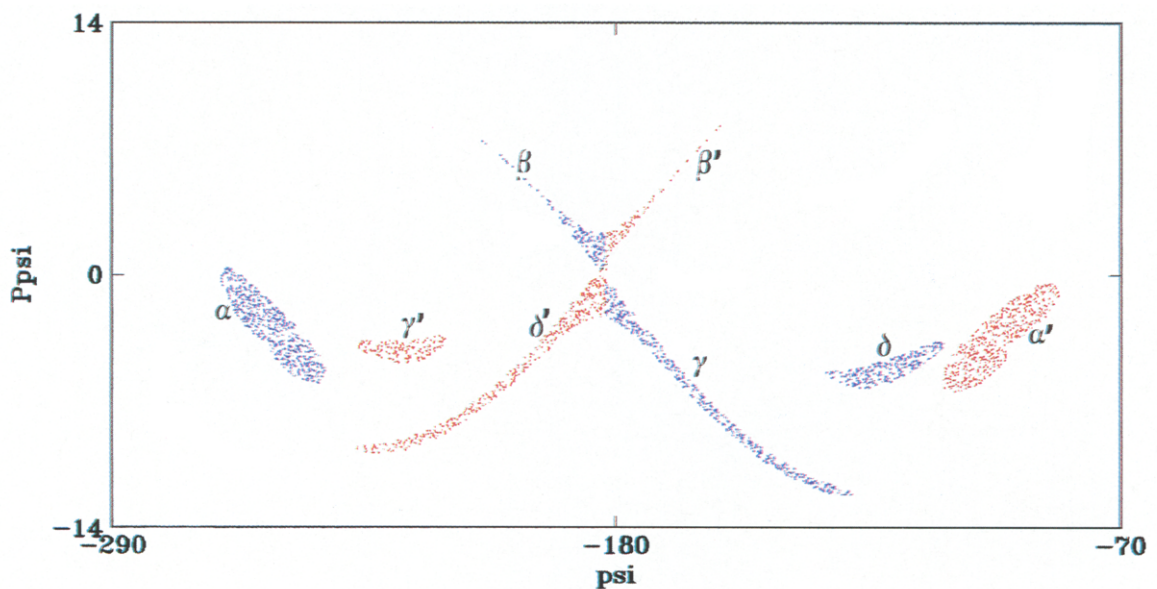
Color Plate 2. Enlarged portion of the antisymmetric modes region of the Poincaré surfaces of section of Color Plate 1 in the  $(\psi, p_\psi)$  plane for energy  $E_T = 2131 \text{ cm}^{-1} = E_A + 99\% E_{\text{esc}} (A \rightarrow B)$  in the vicinity of conformational minimum A of Figure 3.



Color Plate 3(a). Poincaré surfaces of section in the  $(\psi, p_\psi)$  plane for energy  $E_T = 2139 \text{ cm}^{-1} = E_B + 99\% E_{\text{esc}}$  ( $B \rightarrow A$ ) in the vicinity of conformational minimum B of Figure 3. Units are degrees for the abscissa axis and (a.m.u.  $\cdot \text{\AA}^2 \cdot \text{degrees} \cdot \text{fs}^{-1}$ ) for the ordinate axis. (b) Poincaré surfaces of section in the  $(\psi, p_\psi)$  plane for energy  $E_T = 2605 \text{ cm}^{-1} = E_C + 99\% E_{\text{esc}}$  ( $C \rightarrow A$ ) in the vicinity of conformational minimum C of Figure 3. Units are degrees for the abscissa axis and (a.m.u.  $\cdot \text{\AA}^2 \cdot \text{degrees} \cdot \text{fs}^{-1}$ ) for the ordinate axis.



Color Plate 4. Poincaré surfaces of section in the  $(\psi, p_\psi)$  plane for energy  $E_T = 2217 \text{ cm}^{-1} = E_B + 105\% E_{\text{esc}}$  ( $B \rightarrow A$ ) in the vicinity of both conformational minima A and B of Figure 3. Units are degrees for the abscissa axis and (a.m.u.  $\cdot \text{\AA}^2 \cdot \text{degrees} \cdot \text{fs}^{-1}$ ) for the ordinate axis.



Color Plate 5. Reactive islands generated from the Poincaré surfaces of section in the  $(\psi, p_\psi)$  plane for energy  $E_T = 2217 \text{ cm}^{-1} = E_B + 105\% E_{\text{esc}}$  ( $B \rightarrow A$ ) in the vicinity of both conformational minima A and B of Figure 3. Units are degrees for the abscissa axis and (a.m.u.  $\cdot \text{\AA}^2 \cdot \text{degrees} \cdot \text{fs}^{-1}$ ) for the ordinate axis.